ACS OMEGA

Open Access

http://pubs.acs.org/journal/acsodf

Article

Palladium Nanoparticles and Lung Health: Assessing Morphology-Dependent Subacute Toxicity in Rats and Toxicity Modulation by Naringin – Paving the Way for Cleaner Vehicular Emissions

Aarzoo, Mobin A. Siddiqui, Mohammad Hasan, Nidhi, Haider A. Khan, Shweta Rastogi, Indu Arora, and Mohammed Samim*

Cite This: *ACS Omega* 2024, 9, 32745−32759

Read Online

ACCESS | Metrics & More | Article Recommendations | Supporting Information

ABSTRACT: The release of palladium nanoparticles (PdNPs) from autocatalytic converters has raised concerns regarding public health and the environment due to their emergence as anthropogenic contaminants. With growing vehicular population, there is an urgent need for comprehensive toxicological studies of PdNPs to mitigate their risk. The present study aims to investigate the effects of spherical PdNPs with average sizes of 20 and 80 nm, as well as Pd nanorods, on the lung function of female Wistar rats following oral exposure to environmentally relevant doses (1 and 10 μg/kg) over a period of 28 days. Various biological parameters were evaluated, including liver and kidney biochemical changes, lung oxidative stress markers (SOD, CAT, GSH, LPO), lung inflammatory markers (IL-1β, IL-8, IL-6, and TNF-α), and histopathological alterations in the lungs. Additionally, the potential mitigating effects of naringin on PdNPs-induced toxicity were examined. The results demonstrate a significant increase in oxidative stress, the onset of inflammation, and histological changes in lung alveolar sacs upon exposure to all tested particles. Specifically, 20@PdNPs and PdNRs exhibited higher cytotoxicity and pro-inflammatory properties compared to 80@PdNPs. Naringin effectively attenuated the pulmonary toxicity induced by PdNPs by modulating oxidative and inflammatory pathways. These findings contribute to the sustainable development of PdNPs for their future applications in the biomedical and environmental sectors, ensuring the advancement of safe and sustainable nanotechnology.

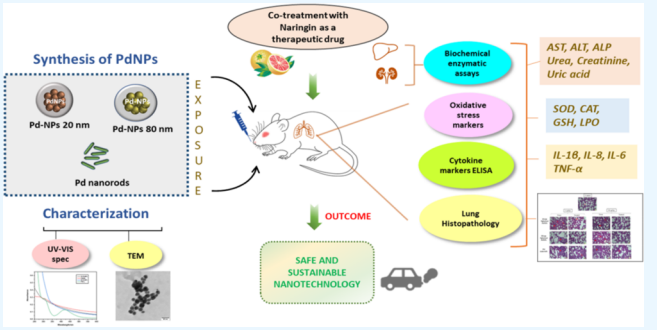

1. INTRODUCTION

Pd is a precious and noble element that belongs to the class of platinum group metals (PGMs) and occurs at a very low concentration (~0.4 ng/g) in the earth's upper continental crust.[1] Because of their outstanding catalytic properties, Pd is extensively utilized in various industrial applications.[2−5] However, its most significant application, comprising over 84% of total Pd usage, lies within the automobile sector as an autocatalyst. Specifically, Pd serves as a crucial component in modern three-way catalytic converters (TWCs) installed in vehicles to reduce air pollution, particularly in mitigating vehicle exhaust emissions.[6]

A TWC consists of a monolithic honeycomb support and has a large catalytic surface area coated with alumina (γ-Al_2O_3) or silica (SiO_2) washcoat. On the catalytic surface, Pd particles of size 0.3 μm down to nanometer (1−100 nm) size range are embedded that act as a catalyst for the conversion of noxious polluted gases such as CO, NO_x, and hydrocarbons into harmless products such as carbon dioxide and water.[7,8] With the enforcement of stringent emission regulations and the rapid expansion of urban areas, the production of Pd-rich three-way catalytic converters (TWCs) has steadily risen.[9,10] However, prolonged exposure to mechanical, chemical, and thermal stresses can cause the catalytic surface of TWCs to corrode and degrade. This deterioration results in the release of fine (≤2.5 μm) and ultrafine (≤100 nm) Pd particles from vehicle exhaust systems into both occupational and living environments, emerging as a novel source of environmental pollution.[8] Consequently, notable levels of Pd have been detected in various environmental compartments, including soil, vegetation, roadside dust, air, sewage, seawater, rainwater, snow, and living organisms.[11−16]

Studies have shown that a significant portion of airborne Pd samples, approximately 30−57%, exists as particulate matter (PM) in the size range of 2.5−10 μm down to nanoparticle size.[17−19] Nanoparticles (1−100 nm) pose a greater risk than

Received: March 20, 2024
Revised: June 28, 2024
Accepted: July 2, 2024
Published: July 16, 2024

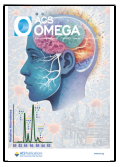

microparticles and have been linked with increased morbidity and mortality.[20,21] These risks stem from their small size, which enables them to penetrate biological barriers and interact with cells and tissues in ways that larger particles cannot. Chronic exposure to nanoparticles has been linked with respiratory, cardiovascular, and neurological diseases. On inhalation, nanoparticles can penetrate deep into the lungs and may cause inflammation and respiratory tract irritation, which may lead to chronic respiratory diseases such as chronic obstructive pulmonary disease (COPD), bronchial asthma (BA), acute respiratory distress syndrome (ARDS), and lung cancer or may exacerbate existing respiratory conditions.[22] Nanoparticles may also enter the bloodstream, either directly or through translocation from other organs, may interact with vascular endothelial cells and contribute to cardiovascular diseases and they may also cross the blood-brain barrier and deteriorate neurological health.[23]

Workers in occupational settings and urban residents face a heightened risk of chronic exposure to palladium nanoparticles (PdNPs) generated by traffic and industrial activities. This exposure occurs primarily through inhalation and ingestion of PdNPs through contaminated food and water sources.[24−28] Air-borne PdNPs upon inhalation may accumulate within the lungs and may enter the bloodstream, influence the immune system, and disseminate throughout the body to target various organs. In this regard, a few *in vitro* studies have observed the effect of PdNPs on exposure to lung cells. For instance, Wilkinson et al. studied dose-dependent effect of PdNPs on primary bronchial epithelial cells (PBEC) and lung epithelial cells (A549). Consequently, PBEC cells were found to exhibit cytotoxicity, increased cellular uptake, and caspase-dependent apoptosis in a dose-dependent manner, while such effects were not observed in A549 cells. Moreover, elevated levels of IL-8 and a reduction in PGE2, an anti-inflammatory marker in airways, were observed indicating an inflammatory response in PBEC cells.[29] In a separate investigation by Ji et al. (2017), 6−10 nm sized PdNPs were introduced to 3D models representing both healthy and chronic bronchitis-like mucosa, constructed using PBEC and fibroblast cells. The results demonstrated a significant rise in IL-8 production in the chronic bronchitis model compared to the normal model, suggesting an exacerbated inflammatory response induced by traffic-related PdNPs.[30] Nevertheless, the current toxicological data remains insufficient, underscoring the necessity for further research into the size and morphology-dependent impact of PdNPs on pulmonary function, particularly in animal models.

When lung cells are exposed to toxic substances such as pollutants, chemicals, or pathogens, they may undergo apoptosis as a protective mechanism to remove damaged cells and prevent further harm to the tissue. Apoptotic cells then trigger an inflammatory response by recruiting immune cells such as macrophages, neutrophils, and lymphocytes. Excessive apoptosis or impaired clearance of apoptotic cells can prolong the inflammatory response, resulting in tissue damage and the development of chronic lung diseases.[31,32] Moreover, different morphologies and sized of PdNPs may exhibit distinct interactions with pulmonary tissues, potentially influencing toxicity profiles. Therefore, understanding the differential effects of PdNPs in relation to their physicochemical properties is crucial as it offers insights into the pathogenesis of lung diseases such as inflammation, oxidative stress, and fibrosis, which are linked with lung diseases such as COPD, bronchial asthma, ARDS, and lung cancer.[22,33]

Therefore, the current study is aimed at the following objectives: (i) synthesis and characterization of spherical PdNPs of mean size ∼20 nm (20@PdNPs), ∼80 nm (80@PdNPs) and Pd nanorods (PdNRs). For the present study, we have selected two distinct size ranges: one falling within a smaller size range (15−30 nm, ∼ 20 nm) and the other encompassing a larger size range (60−100 nm, ∼80 nm) (ii) subacute oral treatment of female Wistar rats with 20@PdNPs, 80@PdNPs, and PdNRs of environmental relevant concentration (1 and 10 μg/kg) for consecutive 28 days; (iii) assessment of size, shape, and dose-dependent liver and kidney toxicity by analyzing their biochemical parameters; (iv) assessment of size, shape, and dose-dependent pulmonary toxicity by estimating oxidative stress and inflammatory markers and by examining histological alterations in lungs; (v) last, modulation of PdNPs' induced toxicity in lungs by using naringin as a therapeutic agent.

2. EXPERIMENTAL SECTION

2.1. Chemicals and Reagents. The chemicals such as palladium(II) chloride (PdCl2, CAS No.: 7647−10−1, ≥ 99.9%), hydrochloride solution (HCl, 0.1 M, CAS No.: 7647−01−0), sodium hydroxide (NaOH; CAS No.: 1310−73−2), sodium borohydride (NaBH4; CAS No.:16940−66−2), cetyltrimethylammonium bromide (CTAB; CAS No.: 57−09−0), silver nitrate (AgNO3; CAS No.: 7761−88−8), ascorbic acid (CAS No.: 50−81−7), sodium citrate tribasic dihydrate ($HOC(COONa)(CH2COONa)_2{\cdot}2H2O$; CAS No.: 6132−04−3), and potassium iodide (CAS No.: 7681−11−0) were purchased from Sigma -Aldrich, USA. Biochemical enzyme assay kits were obtained from Erba Mannheim diagnostics, London, UK. Lastly, ELISA kits were obtained from Abbkine Scientific Co. Ltd., California, USA. All chemicals used were of the highest purity and of analytical grade.

2.2. Synthesis of ∼20 nm Sized Palladium Nanoparticles (20@PdNPs). In a typical synthesis of 20 nm sized-PdNPs (20@PdNPs), 0.01 M H_2PdCl_4 solution was prepared by mixing 0.035 g of $PdCl_2$ salt in 20 mL of Milli Q water and 500 μL of 1 M HCl. Then, 100 μL of H_2PdCl_4 solution was added dropwise to 10 mL of 0.01 M of cetyltrimethylammonium bromide (CTAB) solution and the solution was kept at 60 °C for half an hour. After 30 min, 100 μL of 0.1 M of sodium borohydride ($NaBH_4$) solution was added to the solution and the temperature was raised to 90 °C. The solution was kept on stirring for another 30 min. The change in color from yellow to blackish brown-colored solution indicates the formation of nanopalladium. The solution was cooled down and black-colored particles were collected by centrifuging for 5 min at 7000 rpm. Further, the obtained particles were washed thrice with double distilled water to get rid of the bound surfactant and other impurities and stored at 4 °C.

2.3. Synthesis of ∼80 nm Sized Palladium Nanoparticles (80@PdNPs). In this first report of the typical synthesis of 80 nm sized PdNPs (80@PdNPs), 15 mL of 5×10^{-3} M solution of sodium borohydride was mixed with 30 mL of 2×10^{-3} M of trisodium citrate tribasic dihydrate solution (TSC) and was stirred vigorously at 60 °C to obtain a homogeneous solution. After 30 min of stirring, 5 mL of 2×10^{-3} M H_2PdCl_4 solution was added dropwise to the obtained clear solution and the temperature was raised to 90 °C. After 20 min of stirring, 100 μL of 0.1 M of NaOH was added to maintain the pH at 10.5. The solution was stirred for a further

https://doi.org/10.1021/acsomega.4c02269
ACS Omega 2024, 9, 32745−32759

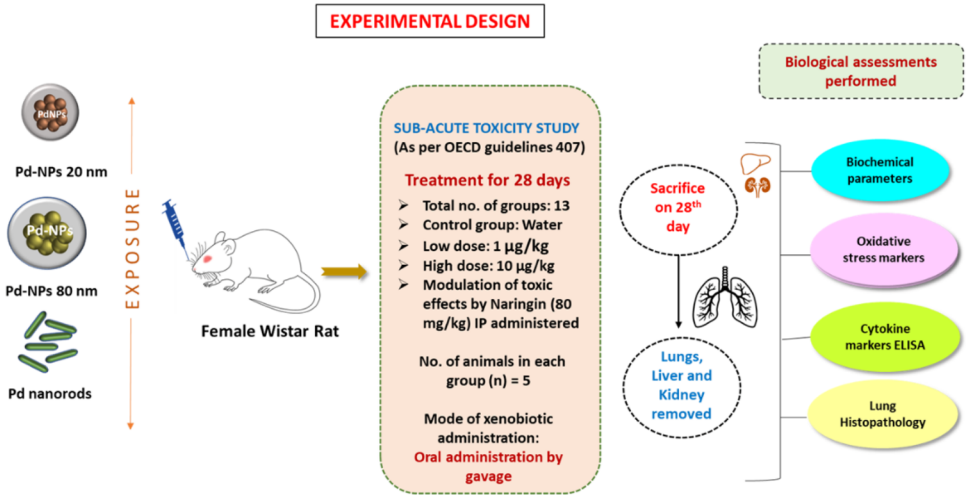

Figure 1. Overview of the experimental study design.

20 min until a color change was observed. The color of the reaction was changed from pale yellow color to dark brown color indicating the formation of nanoparticles. The solution was left to cool down and then suspended particles were centrifuged for 10 min at 7000 rpm and the black-colored particles were collected. The particles were further purified by washing the particles thrice with double distilled water and then stored at 4 °C.

2.4. Synthesis of Palladium Nanorods (PdNRs). Palladium nanorods (PdNRs) were synthesized by using a seedless reduction method performed according to Tang et al. with certain modifications.[34] In a typical synthesis, 600 μL of 0.0l M of yellow-colored H_2PdCl_4 solution was added dropwise to 20 mL of 100 mM of cetyltrimethylammonium bromide (CTAB) solution and the solution was kept at 90 °C for 1 h on the magnetic stirrer with minimal stirring. After 1 h, 400 μL of freshly prepared 0.1 M KI and 160 μL of 0.01 M $AgNO_3$ salt were added to the solution in sequence and the color of the solution immediately changed from yellow to reddish-orange. After 5 min of stirring, 400 μL of 0.1 M of freshly prepared ascorbic acid (AA) was added and the reaction mixture was stirred for another 1 h at 90 °C. After 1 h of heating, the color of the solution gradually changed from reddish-orange to blackish-brown colored solution, which indicated the formation of Pd nanorods. The black-colored nanorods were collected in a separate vial by centrifuging the solution for 15 min at 7000 rpm. The precipitate was further purified by washing the nanorods thrice with ethanol and water.

2.5. Characterization of PdNPs. 20@PdNPs, 80@PdNPs, and PdNRs were characterized by estimating the characteristic absorption peak through a double beam Halo DB-20R UV−vis spectrophotometer with a 1 cm quartz cell and between 200 and 500 nm absorption wavelength range. For the morphological analysis, high-resolution transmission electron microscopy was carried out on a TEM instrument (Thermo Fisher Scientific, Talos L120C) at 100 keV. The size distribution histogram of PdNPs was plotted with the help of Origin Pro 2022 and ImageJ software.

2.6. Test Animals. For the present study, 65 healthy female Wistar albino rats of 7−8 weeks, each weighing between 180 and 250 g, were procured from the Central Animal House Facility of Jamia Hamdard, New Delhi. Wistar rats are an outbred strain of albino rats, which are generally used as a multipurpose model in medical and biomedical research.[35] The use of rats offers multiple advantages such as similar metabolic pathways to humans, similar anatomical and physiological characteristics, and large literature for comparative purposes. Female Wistar rats were chosen for the present subacute toxicity study because according to Pd sensitization studies on urban population, there have been a rising number of positive patch test results year by year, among which the female sex was the most affected.[36,37] Also, in previous in vivo toxicity studies, the female Wistar rats model has been used for investigating the impact of PdNPs on cytokine serum levels and renal function.[38,39] The animals were housed in standard plastic cages and were allowed to acclimatize under standard experimental conditions, i.e., 12 h light/dark cycle at a temperature of 23 ± 2 °C with a relative humidity of 50 ± 10% prior to 1 week of the experiment. The rats were supplied a standard pellet diet and water *ad libitum*.

2.7. Ethical Statement for the *In Vivo* Study. The experimental protocol and treatments were approved by the Institutional Animal Ethics Committee (IAEC) of Jamia Hamdard, New Delhi, India (Approval No.1562, registration No. 173/GO/ReBi/S/2000/CPCSEA). All experiments were performed in compliance with the relevant laws of India and institutional guidelines (CPCSEA, IAEC). All rats were handled ethically according to the standard guide for the care and use of laboratory animals.

2.8. Experimental Design. *2.8.1. Animal Grouping.* To study the effect of 20@PdNPs, 80@PdNPs, and PdNRs on the pulmonary function of female Wistar rats in a subacute toxicity study, sixty-five rats were weighed and randomly divided into 13 groups with five animals (n = 5) in each group as follows:

- **Group 1**: control, exposure to 1 mL of water
- **Group 2**: exposure to 1 μg/kg of PdNPs of size 20 nm (20@PdNPs-1)
- **Group 3**: exposure to 10 μg/kg of PdNPs of size 20 nm (20@PdNPs-10)
- **Group 4**: exposure to 1 μg/kg of PdNPs of size 80 nm (80@PdNPs-1)
- **Group 5**: exposure to 10 μg/kg of PdNPs of size 80 nm (80@PdNPs-10)
- **Group 6**: exposure to 1 μg/kg of Pd nanorods (PdNRs-1)

https://doi.org/10.1021/acsomega.4c02269
ACS Omega 2024, 9, 32745−32759

- **Group 7**: exposure to 10 μg/kg of PdNRs (PdNRs-10)
- **Group 8**: exposure to 1 μg/kg of PdNPs 20 nm + Naringin (80 mg/kg body weight)
- **Group 9**: exposure to 10 μg/kg of PdNPs 20 nm + Naringin (80 mg/kg body weight)
- **Group 10**: exposure to 1 μg/kg of PdNPs 80 nm + Naringin (80 mg/kg body weight)
- **Group 11**: exposure to 10 μg/kg of PdNPs 80 nm + Naringin (80 mg/kg body weight)
- **Group 12**: exposure to 1 μg/kg of PdNRs + Naringin (80 mg/kg body weight)
- **Group 13**: exposure to 10 μg/kg of PdNPs + Naringin (80 mg/kg body weight)

The overview of the experimental study design is displayed in Figure 1.

2.8.2. Dose Administration. To assess the impact of 20@PdNPs, 80@PdNPs, and PdNRs on pulmonary, hepatic, and renal function in animals, a repeated dose 28-day subacute oral toxicity study was conducted following OECD guideline 407 (Test No. 407). Sixty-five rats were randomly divided into 12 exposure groups and one control group, with five rats per group (n = 5). The rats in the exposure groups (groups 2−7) were orally administered repeated doses of water (negative control group), as well as different concentrations of PdNPs and PdNRs (1 μg/kg and 10 μg/kg) via oral gavage for consecutive 28 days.

The doses of PdNPs at their respective concentrations were prepared by suspending the required amount of PdNP solid powder in an aqueous solution. The oral route of administration was chosen for PdNPs, as it is assumed that individuals might be exposed to PdNPs through ingesting food and water contaminated with these particles. In this study, two environmentally relevant doses were selected: 1 and 10 μg/kg, to mimic possible occupational and living environment exposure scenarios. Literature reports have indicated a highest mean Pd airborne level of 7.7 ± 4.15 μg/m^3 in occupational settings.[40] Considering a human breathing rate of 20 m^3/day and an average body weight of 70 kg, potential occupational exposure via inhalation to PdNP corresponds to 2.2 μg/kg.[38,41] The higher dose (10 μg/kg) was chosen to simulate potential occupational exposure under normal and accidental conditions where re-exposure may occur. The lower dose (1 μg/kg) was chosen to simulate exposure levels resembling those of the general population living near highways. Studies have reported Pd levels ranging from 1 to 1000 μg/kg in road dust and roadside soil.[42−44] Therefore, the selected doses in this study resemble occupational and environmental exposure scenarios.

The remaining six groups (groups 8−13) were cotreated with naringin (80 mg/kg) through intraperitoneal (IP) administration as a protective drug to modulate toxicity. Naringin, a flavanone-7-*O*-glycoside belonging to the family of flavonoids, is naturally found in citrus fruits such as grapefruits.[45] Previous studies have established that naringin exhibits strong antioxidant and anti-inflammatory activities against pulmonary fibrosis by upregulating antioxidant enzymes and suppressing inflammatory markers such as TNF-α.[46,47] Thus, naringin is expected to serve as an effective therapeutic agent, providing protection against pulmonary fibrosis and toxicity induced by PdNPs. The therapeutic effects of naringin have been demonstrated in a dose range of 60−120 mg/kg in previous studies.[46,47] Therefore, an 80 mg/kg dose of naringin was chosen for toxicity attenuation in this study.

2.8.3. Biological Sample Preparation. At the end of the 28th day of the experiment, the rats were fasted overnight and sacrificed using diethyl ether as anesthesia. Subsequently, the blood samples were collected by cardiac puncture and collected in clean tubes containing heparin as an anticoagulating agent and immediately placed on crushed ice in a box. The plasma serum was obtained from blood by centrifuging the vials at 3500 rpm for 15 min at 4 °C and kept at −80 °C for further analysis of various biochemical parameters of the liver and kidney. Immediately, the lungs were removed from the body, washed with a chilled saline solution followed by the removal of their connective tissues, and fat adhered to the organ tissue. The tissue samples from the lung were stored in cold phosphate-buffered saline (PBS) solution (10% w/v) and homogenized using a homogenizer machine. The homogenized solution was centrifuged at 10,000g for 20 min at 4 °C and the obtained clear supernatant was collected for further analysis of biochemical assays such as oxidative stress markers and inflammatory markers analysis. The remaining tissue samples were fixed in a 10% neutral buffered formalin solution for histopathology processing. Protein estimation was performed by the methodology given by lowry et al. (1951) using bovine serum albumin (BSA) as a protein standard.[48]

2.9. Clinical Signs and Body Weight. To examine the effect of exposure to 20@PdNPs, 80@PdNPs, and PdNRs on female Wistar rats, their clinical signs such as changes in the skin, fur, nasal secretions, excretions, locomotive behavior, the occurrence of skin lesions, respiratory pattern and signs of unusual behavior such as repetitive circling, posture, irritability, and self-mutilation were observed. The body weights of animals were noted down once before the treatment (day 0) and then on the weekly basis after the onset of the treatment for 4 weeks.

2.10. Biochemical Parameters. Various liver enzymatic and protein assays such as bilirubin levels, alanine transaminase (ALT), aspartate transaminase (AST), alkaline phosphate (ALP), total protein, albumin, globulin, and kidney biochemical assays such as urea, creatinine, uric acid, sodium, potassium, and chloride were performed by analyzing the blood serum obtained from cardiac puncture approach as per the instructions provided by reagent kits (Erba Mannheim diagnostics, London, UK).

2.11. Markers of Oxidative Stress. Enzymatic and nonenzymatic antioxidant assays such as superoxide dismutase activity (SOD), catalase activity (CAT), lipid peroxidation (LPO) test, and reduced glutathione (GSH) tests were performed according to the protocol available in the Supporting Information (Section S1). Protein estimation was performed by the methodology given by Lowry et al. (1951) using Bovine Serum Albumin (BSA) as a protein standard.[48]

2.12. Inflammatory Markers Estimation Using ELISA. The levels of interleukin (IL-6, IL-8, IL-1β) and tumor necrosis factor (TNF-α) in lung tissue homogenates of each group were detected and quantified by enzyme-linked immunosorbent assay (ELISA) kits containing dyed microspheres conjugated with a monoclonal antibody specific for a target protein (Abbkine Scientific Co. Ltd., California, USA) using a serial standard dilution procedure for each parameter as per the manufacturer's instructions. Detailed protocol for estimating cytokines using ELISA is provided in the Supporting Information, S2. Cytokine levels were detected using an Alere ELISA microplate reader (Alere AM 2100).

https://doi.org/10.1021/acsomega.4c02269
ACS Omega 2024, 9, 32745−32759

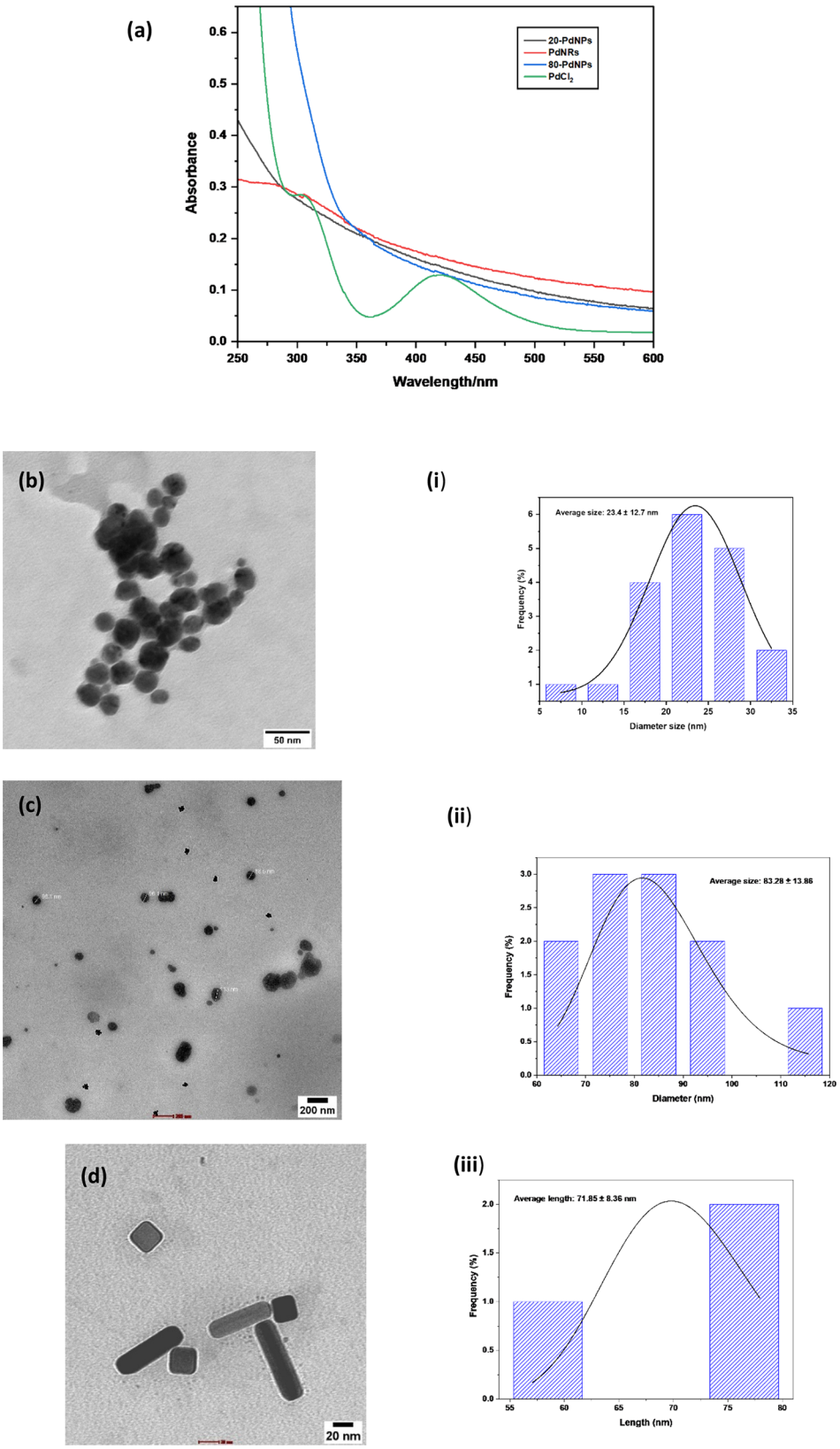

Figure 2. (a) Ultraviolet−visible (UV−vis) spectra of palladium chloride salt, $PdCl_2$ (green line), PdNPs of size 20 nm, 20-PdNPs (black line), PdNPs of size 80 nm, 80-PdNPs (blue line) and palladium nanorods, PdNRs (red line). (b−d) High resolution transmission electron microscopy of (b) 20@PdNPs, (c) 80@PdNPs, and (d) PdNRs and figures (i−iii) shows the corresponding histogram of size distribution analysis of particles.

2.13. Lung Histopathology Analysis. For histopathological analysis of lung tissues, lung samples collected from the animals of all groups were fixed in 10% neutral buffered formalin for 48 h, then dehydrated using ethanol, and further cleared with xylene. The dehydrated clean samples were embedded in paraffin after 24 h and cut into 5 μm sections.

https://doi.org/10.1021/acsomega.4c02269
ACS Omega 2024, 9, 32745−32759

Figure 3. Lesions and wounds on the skin of female Wistar rats after the onset of the third week of exposure to PdNPs.

Lastly, the tissue sections were stained using hematoxylin and eosin (H&E) dye as previously described.[49,50] A light microscope (Olympus BH-2, Japan) was used for further analysis of any pathological changes in the lungs.

2.14. Statistical Analysis. All the experiments were done in triplicate and data was expressed as mean ± standard deviation (SD). The statistical differences between control and treated groups were analyzed using a two-way ANOVA analysis of variance and were followed by post hoc multi-comparison Tukey's test. The difference was considered statistically significant at a P value <0.05. The graphs were plotted with the help of GraphPad prism ver. 9.3.1 software (San Diego, CA, USA) and Origin Pro 2022 (version: 9.9.0.225).

3. RESULTS AND DISCUSSION

3.1. Characterization of PdNPs. *3.1.1. UV−vis Spectroscopy.* To confirm the formation of colloidal 20PdNPs, 80PdNPs, and PdNRs, ultraviolet−visible (UV−vis) spectroscopy technique was conducted in the wavelength range of 250−600 nm using a Halo DB-20R UV−vis spectrophotometer. The obtained UV−vis spectra were compared with the UV−vis spectrum of a $PdCl_2$ solution (Figure 2a).

The UV−vis spectrum of $PdCl_2$ exhibited a maximum absorbance (λmax) at approximately 425 nm (400−450 nm), which is known as the characteristic peak of Pd^{2+} ions.[42,51,52] This peak is attributed to electronic d-d transition in Pd^{2+} ions with a d^8 electron configuration. In contrast, the UV−vis spectra of 20@PdNPs, 80@PdNPs, and PdNRs displayed a different pattern. The characteristic peak of Pd^{2+} ions at around 425 nm was absent, and a linear curve was observed instead, indicating the formation of PdNPs in their zerovalent state (Pd^0). This observation is consistent with previous studies.[42,52,53] The disappearance of the characteristic Pd^{2+} peak and the emergence of a linear curve in the UV−vis spectra further confirm the successful formation of PdNPs in colloidal form.

3.1.2. Surface Morphology and Size Distribution Analysis. Surface morphology and size distribution analysis of the synthesized 20@PdNPs, 80@PdNPs, and PdNRs were performed using transmission electron microscopy (TEM). TEM images of the particles and their corresponding size distribution histograms are presented in Figure 2b−d and Figure 2i−iii.

To synthesize 20@PdNPs, CTAB was used as a capping agent, and $NaBH_4$ served as a reducing agent. This method resulted in the formation of slightly poly dispersed spherical particles with an average size of approximately 23.4 ± 12.7 nm (∼20 nm), as shown in Figure 2b and Figure 2i. The polydispersity index was determined to be 0.5, indicating a moderate level of size variation.

For the synthesis of 80@PdNPs, TSC was employed as a capping agent, and NaBH4 was used as a strong reducing agent. This method yielded monodispersed spherical particles with an average size of approximately 83.2 ± 13.8 nm (∼80 nm), as depicted in Figure 2c and Figure 2ii. The polydispersity index for these particles was found to be 0.15, indicating a relatively narrow size distribution.

Pd nanorods were synthesized using a seedless method, where CTAB served as a cationic surfactant and ascorbic acid acted as a reducing agent. This approach resulted in the formation of penta-twinned Pd nanorods with an average length of approximately 71.8 ± 8.3 nm, exhibiting distinct rod-shaped structures. The polydispersity index for the Pd nanorods was determined to be 0.1, indicating a relatively uniform size distribution, as shown in Figure 2c and Figure 2iii.

3.2. Results of *In Vivo* Subacute Toxicity Study and Toxicity Modulation by Naringin. *3.2.1. The Appearance of Clinical Signs and Changes in Body Weight.* The appearance of clinical signs is a valuable indicator to study the potential toxicity risks caused by xenobiotics. In the present study, the rats were observed for behavioral changes, respiratory distress, neurological changes, and dermatological changes for a period of 28 days on exposure to PdNPs. Behavioral changes such as hyperactivity, lethargy, or agitation were observed. In the initial 2 weeks, no abnormal locomotive behavior, or unusual behaviors such as repetitive circling or changes in posture were observed. No unusual respiratory pattern such as unusual wheezing, coughing or nasal secretions were observed. No signs of neurotoxicity such as tremors, paralysis or seizures were observed. There were no instances of mortality among the rats during the 28-day duration. During the third week, rats administered with an oral dose of 10 μg/kg of both 20@PdNPs and 80@PdNPs exhibited skin lesions. Notably, the severity of these lesions was more pronounced in the 20@PdNPs-treated group compared to the 80@PdNPs-treated group. Moreover, heightened irritability and frequent itching were also noted. These observed side effects are likely associated with Pd sensitization, given its potent capacity to induce allergic contact dermatitis (Figure 3).

The body weight of rats in each group was measured on day 0, day 7, day 14, day 21, and day 28 (Figure 4). The initial body weight of the control group (group 1) on day 0 was recorded as 211.3 ± 10.5 g, and the final body weight on day

https://doi.org/10.1021/acsomega.4c02269
ACS Omega 2024, 9, 32745−32759

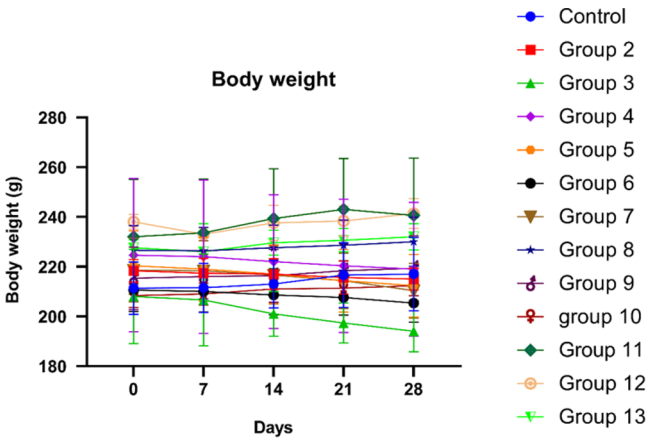

Figure 4. Body weight of female Wistar rats after subacute oral treatment with PdNPs of different sizes, shapes, and concentrations for 28 days. Each data represents as mean ± SD (n = 5).

28 was 217 ± 14.7 g. The control group exhibited a gradual increase in body weight over the course of the study. However, compared to the control group, a gradual decrease in body weight was observed in rats from group 2 to group 7. Specifically, rats given high oral doses (10 μg/kg) of PdNPs showed a greater decrease in weight compared to those given lower doses of Pd particles, indicating a significant impact on body weight. The decrease in body weight was most pronounced in group 3 rats (20@PdNPs, 10 μg/kg) compared to the other groups. On the other hand, animals in groups 8 to 13 that were treated with naringin displayed relatively stable or slightly increased body weights, similar to the control group. However, no statistically significant differences were observed in any of the cases (Table 1).

3.2.2. Alterations in Biochemical Parameters. The ingestion of xenobiotics can cause alterations in liver and kidney enzyme levels, necessitating the evaluation of biochemical parameters to determine the metabolic health of animals. Liver function was assessed through the analysis of parameters such as total bilirubin, direct and indirect bilirubin, aspartate transaminase (AST), alanine aminotransferase (ALT), alkaline phosphatase (ALP), total protein, albumin, and globulin levels (Table 2). Significant changes were observed in these parameters in all groups compared to the control, indicating liver dysfunction. Particularly, rats exposed to higher doses of 10 μg/mL of 20@PdNPs, 80@PdNPs, and PdNRs exhibited significantly elevated total bilirubin levels (p < 0.01). Group 3 rats treated with 10 μg/kg of 20@PdNPs showed the highest increase in direct bilirubin levels, suggesting possible hepatocellular injury due to higher doses.

ALP, AST, and ALT are vital markers for evaluating hepatic injury resulting from xenobiotic exposure. In this study, a highly statistically significant increase in AST levels (p < 0.001) was observed in group 3 rats treated with 10 μg/kg of 20@PdNPs compared to the control group. Similarly, group 7 rats treated with 10 μg/kg of PdNRs exhibited a significant rise in AST values compared to the control group (p < 0.01). ALT levels followed a similar trend, with group 3 and group 7 rats showing significantly higher values than the control (p < 0.01). Likewise, ALP levels showed a significant increase in higher doses compared to the control group. Notably, group 3 rats treated with 10 μg/kg of 20@PdNPs exhibited the highest ALP levels (p < 0.01) among the studied groups.

Kidney function was assessed by analyzing parameters such as urea, creatinine, uric acid, sodium, potassium, and chloride levels. Urea, creatinine, and uric acid are essential markers for evaluating kidney health (Table 3). In this study, a significant increase in urea levels compared to the control group was observed in groups administered a daily dose of 10 μg/kg of 20@PdNPs and 80@PdNPs and PdNRs (p < 0.05). Similarly, high creatinine levels were observed in all groups compared to the control group, with significant changes in group 3 rats (20@PdNPs, 10 μg/kg), group 6 rats (PdNRs, 1 μg/kg), and group 7 rats (PdNRs, 10 μg/kg) (p < 0.05). Elevated levels of uric acid were also observed in all groups compared to the control group, with significant changes in group 3 rats (20@PdNPs, 10 μg/kg), group 5 rats (80@PdNPs, 10 μg/kg), and group 7 rats (PdNRs, 10 μg/kg). However, the changes in sodium, potassium, and chloride levels were not found to be significant.

In conclusion, the increased levels of liver and kidney enzymes indicate hepatic and renal impairment caused by the toxicity induced by palladium nanoparticles. Furthermore, the study demonstrates the impact of varying sizes and shapes of metal particles on these biochemical parameters, emphasizing the importance of careful evaluation in toxicological studies.

Table 1. Body Weight of Female Wistar Rats after Subacute Oral Treatment with PdNPs of Different Sizes, Shapes, and Concentration for 28 Days[a]

group	day 0	day 7	day 14	day 21	day 28
group 1 (Control)	211.3 ± 10	211.5 ± 10	213 ± 9.5	216.6 ± 13	217 ± 15
group 2 (PdNPs, ∼ 20 nm, 1 μg/kg)	218.3 ± 4.5	217.3 ± 6	217 ± 6.2	215.6 ± 7	215 ± 4
group 3 (PdNPs, ∼ 20 nm, 10 μg/kg)	208 ± 19	206.6 ± 18	201 ± 9	197.3 ± 8	194 ± 8
group 4 (PdNPs, ∼ 80 nm, 1 μg/kg)	225 ± 30	224 ± 31	222 ± 27	220 ± 26	219 ± 27
group 5 (PdNPs, ∼ 80 nm, 10 μg/kg)	220.3 ± 14	219 ± 13	217 ± 12	214 ± 13	212 ± 12
group 6 (PdNRs, 1 μg/kg)	211 ± 9	210 ± 8	209 ± 8	208 ± 7	205 ± 8
group 7 (PdNRs, 10 μg/kg)	219 ± 13	218.3 ± 12	217 ± 12	214 ± 11	210 ± 11
group 8 (20@PdNPs+ Nar, 1 μg/kg)	227 ± 10	226.3 ± 9	228 ± 9	229 ± 10	230 ± 10
group 9 (20@PdNPs + Nar, 10 μg/kg)	215.3 ± 13	216 ± 9	216 ± 10.5	218 ± 11	219 ± 13
group 10 (80@PdNPs + Nar, 1 μg/kg)	208.3 ± 5	209 ± 4.3	211 ± 5	211 ± 4	212 ± 4
group 11 (80@PdNPs + Nar, 10 μg/kg)	232 ± 3	233 ± 10	239 ± 12	243 ± 5	241 ± 13
group 12 (PdNRs + Nar, 1 μg/kg)	238 ± 3	233 ± 3	238 ± 7	238 ± 6	241.3 ± 6
group 13 (PdNRs + Nar, 10 μg/kg)	228 ± 3.2	226 ± 10	230 ± 5	231 ± 4.7	232 ± 5

[a]Each data represents as mean ± SD. Two way-ANOVA, Tukey's multiple comparison test. No statistically significant difference was observed.

https://doi.org/10.1021/acsomega.4c02269
ACS Omega 2024, 9, 32745−32759

Table 2. Changes in the Biochemical Activity of Liver after 28-Day Subacute Oral Treatment of PdNPs of Different Sizes, Shapes, and Concentrations[a]

	experimental groups						
parameter	control (group 1)	20@PdNPs, 1 μg/kg (group 2)	20@PdNPs, 10 μg/kg (group 3)	80@PdNPs, 1 μg/kg (group 4)	80@PdNPs, 10 μg/kg (group 5)	Pd-NRs, 1 μg/kg (group 6)	Pd-NRs, 10 μg/kg (group 7)
total bilirubin (mg/dL)	0.8 ± 0.03	2.5 ± 0.1**	3 ± 0.01	3 ± 0.04	3.2 ± 0.02	2 ± 0.14*	3.1 ± 0.01
direct bilirubin (mg/dL)	0.2 ± 0.03	1 ± 0.1*	2 ± 0.02	1.7 ± 0.04**	2.1 ± 0.01	1 ± 0.04*	1.9 ± 0.03***
indirect bilirubin (mg/dL)	0.6 ± 0.01	1.6 ± 0.02	1.2 ± 0.01	1.2 ± 0.04**	1.1 ± 0.09*	1 ± 0.02**	1.2 ± 0.03
AST (U/L)	203 ± 8	277.4 ± 0.8*	301 ± 66.1***	238 ± 3*	244 ± 2*	248 ± 1.7*	284 ± 2.2**
ALT (U/L)	71 ± 6	151 ± 16*	173 ± 2**	146 ± 2**	138 ± 3	134 ± 1*	168 ± 2**
alkaline phosphatase (ALP) (U/L)	78 ± 2	117 ± 28*	172 ± 10.5**	152 ± 0.8*	153 ± 1.8*	146 ± 7*	168 ± 37**
total protein (g/dL)	3.2 ± 0.1	3 ± 0.1	3 ± 0.1*	2.5 ± 0.07*	3 ± 0.2	4.2 ± 0.1	2.7 ± 0.09
albumin (g/dL)	1.8 ± 0.2	0.8 ± 0.05	1.4 ± 0.08	1.3 ± 0.30	1.5 ± 0.02	1.7 ± 0.8	1.2 ± 0.03
globulin (g/dL)	1.4 ± 0.08	1.8 ± 0.03	1 ± 0.03	1.3 ± 0.04	1.2 ± 0.01	2.5 ± 0.1*	1.5 ± 0.2

[a]Untreated cells were treated as control. Data is expressed as mean ± SD. Asterisk (*) represents significant differences. Two way-ANOVA, Tukey's multiple comparison test. *Significance of $p < 0.05$, **significance of $p < 0.01$, ***significance of $p < 0.001$.

Table 3. Changes in the Biochemical Activity of the Kidney after 28-Day Subacute Oral Treatment of PdNPs of Different Sizes, Shapes, and Concentrations[a]

	experimental groups						
parameter	control (group 1)	20@PdNPs, 1 μg/kg (group 2)	20@PdNPs, 10 μg/kg (group 3)	80@PdNPs, 1 μg/kg (group 4)	80@PdNPs, 10 μg/kg (group 5)	PdNRs, 1 μg/kg (group 6)	PdNRs, 10 μg/kg (group 7)
urea (mg/dL)	32 ± 2	34 ± 1.4	42 ± 2*	36 ± 2	42.3 ± 3*	39.3 ± 4	44 ± 1.6*
creatinine (mg/dL)	0.3 ± 0.1	0.5 ± 0.1	0.7 ± 0.16*	0.4 ± 0.1	0.5 ± 0.1	0.9 ± 0.2*	0.8 ± 0.03*
uric acid (mg/dL)	3 ± 0.2	6.5 ± 0.8*	13 ± 1**	9.5 ± 0.8*	10.4 ± 2*	9.3 ± 0.1*	11 ± 1.5*
sodium (mmol/L)	137 ± 4	139 ± 4	136 ± 3.5	139 ± 3.6	138 ± 2.5	135 ± 3	137 ± 4.3
potassium (mmol/L)	8.4 ± 0.9	12 ± 0.5	11 ± 1.5	12 ± 0.5	12 ± 0.5	12.3 ± 0.8	12.4 ± 0.8
chloride (mmol/L)	110 ± 5.5	117 ± 2	116 ± 4	118 ± 7	118 ± 3	118 ± 3	117 ± 3.2

[a]Untreated cells were treated as control. Data is expressed as mean ± SD. Asterisk (*) represents significant differences. Two way-ANOVA, Tukey's multiple comparison test. *Significance of $p < 0.05$, **significance of $p < 0.01$, ***significance of $p < 0.001$.

3.2.3. Alterations in Oxidative Stress Parameters and Treatment with Naringin. Reactive oxygen species (ROS) and oxidative stress play a significant role in the pathogenesis of lung diseases such as COPD, asthma, and pulmonary fibrosis.[54] Oxidative stress can result from exposure to air pollutants causing damage to cellular components and exacerbating inflammation. Oxidative stress arises from an imbalance between reactive species and antioxidants in the system.[55] In our study, we assessed four crucial oxidative stress markers: superoxide dismutase (SOD), catalase (CAT), lipid peroxidation (LPO), and glutathione (GSH).

SOD is an important enzymatic antioxidant that acts as the first line of defense against free radicals and reactive oxygen species (ROS). It reduces the levels of O^{2-} by converting it into hydrogen peroxide (H_2O_2) and molecular oxygen within the cell mitochondria.[56] Figure 5A demonstrates a significant decrease in SOD activity in rats treated with higher doses (10 μg/kg) of PdNPs and PdNRs ($p < 0.001$). Among them, 20@PdNPs showed the greatest depletion of SOD levels, indicating higher oxidative damage and suppression of antioxidant defenses upon uptake by pneumocytes compared to 80 nm-sized and rod-shaped nanoparticles. However, the coadministration of low and high doses of 20@PdNPs, 80@PdNPs, and PdNRs with naringin led to a noticeable reduction in oxidative damage to lung cells by significantly improving cellular antioxidant potential.

Figure 5B presents the catalase activity in lung tissues, indicated by the consumption of hydrogen peroxide in μmoles per minute per milligram of protein. Catalase acts as an antioxidant enzyme that mitigates oxidative stress by converting harmful cellular hydrogen peroxide into water and oxygen. A decrease in catalase levels in lung tissue indicates excessive generation of ROS, while an increase indicates a healthy defense system against ROS species. In our study, the decrease in catalase levels was more significant ($P < 0.01$) in rats treated with 10 μg/kg of PdNPs compared to those treated with 1 μg/kg ($P < 0.05$) and the control group. Among the 20@PdNPs, 80@PdNPs, and PdNRs, 20@PdNPs showed the lowest antioxidant activity, while 80@PdNPs showed the highest, although no significant difference was observed among all three. Co-treatment with Naringin resulted in a drastic improvement in antioxidant activity, surpassing even the control group, indicating the revival of the antioxidant defense system.

Glutathione (GSH), a nonenzymatic low-molecular antioxidant, plays a crucial role in scavenging reactive oxygen species (ROS) and reactive nitrogen species (RNS) due to its thiol (-SH) moiety.[57] GSH exists in oxidized (GSSG) and

https://doi.org/10.1021/acsomega.4c02269
ACS Omega 2024, 9, 32745−32759

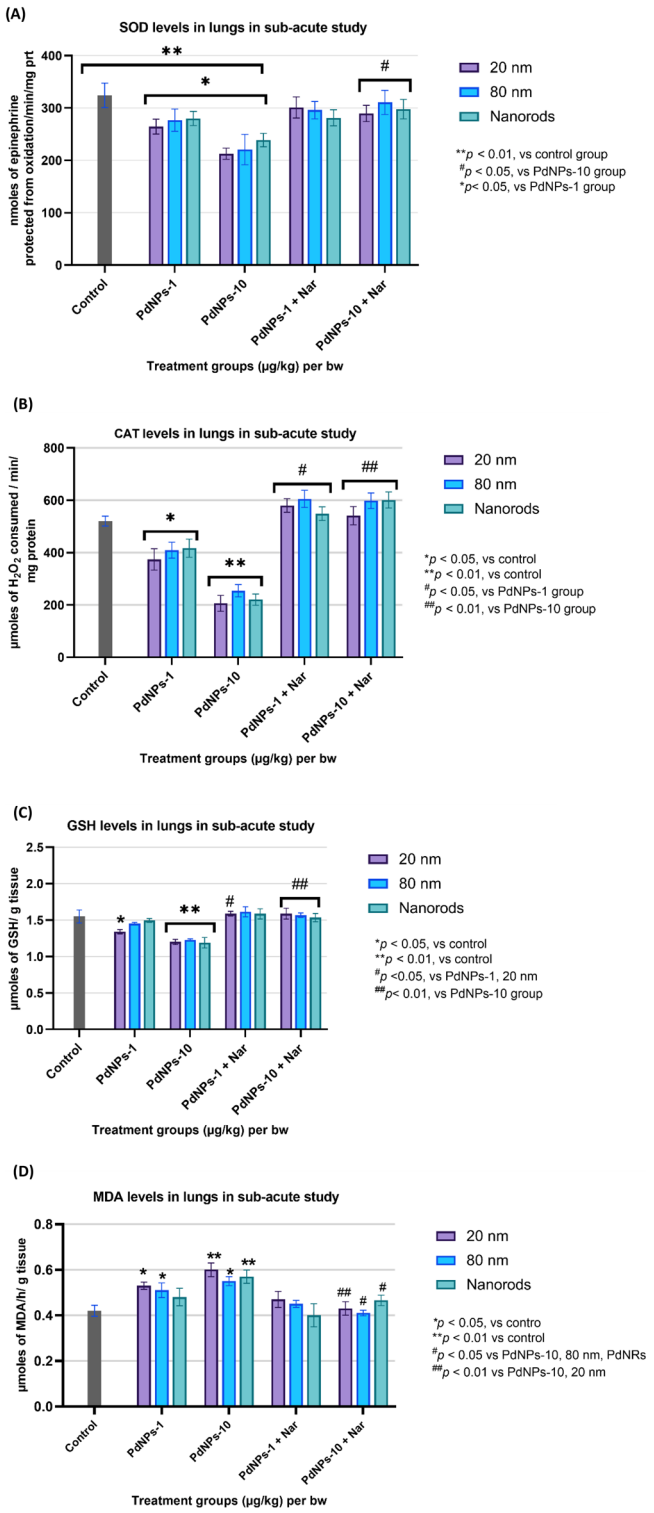

Figure 5. Alteration in enzymatic and nonenzymatic antioxidant activity in lung tissue of rats after 28 days of subacute oral treatment with PdNPs of different sizes, shapes, and concentrations and cotreatment with naringin. (A) SOD activity in lungs, (B) CAT activity in lungs, (C) GSH levels in lungs, and (D) MDA levels in lungs. Untreated cells were taken as control. Data are expressed as mean ± SD (n = 5). Asterisk (*) represents significant differences. Two way-ANOVA, Tukey's multiple comparison test.

reduced forms, with the reduced form being predominant. An increase in the GSSG:GSH ratio and a decrease in GSH activity levels indicate severe oxidative stress.[58] As shown in Figure 5C, a significant decline in GSH levels was observed in rats treated with 1 μg/kg of 20@PdNPs ($P < 0.05$) compared to the control group, while rats treated with 1 μg/kg of 80@PdNPs and PdNRs did not exhibit significant changes. In rats treated with 10 μg/kg, a significant decrease in GSH levels was observed for all three types of nanoparticles compared to the control group ($P < 0.01$). However, cotreatment with low and high doses of 20@PdNPs, 80@PdNPs, and PdNRs, along with naringin, resulted in a replenishment of GSH levels.

Lipid peroxidation, an important consequence of nanoparticle-induced cytotoxicity, serves as a key oxidative stress biomarker. The peroxidation of membrane lipids by reactive species can lead to a loss of membrane flexibility, increased cellular fluidity, and eventual cell death.[59] Malondialdehyde (MDA) levels, the end-product of lipid peroxidation, are used to estimate the extent of lipid peroxidation. Figure 5D displays MDA levels in lung tissues from our subacute study. A significant increase in MDA levels compared to the control group was observed in rats treated with 1 μg/kg of 20@PdNPs and 80@PdNPs ($P < 0.05$). In rats treated with 10 μg/kg of PdNPs, enhanced levels of MDA were observed for all three types of particles, with the most significant effect seen in rats treated with 20@PdNPs ($P < 0.01$). Co-administration of naringin in rats treated with 1 μg/kg of PdNPs led to a decrease in MDA levels compared to the group given the 1 μg/kg dose alone, although the decrease was not statistically significant. In the case of rats treated with 10 μg/kg of PdNPs and cotreated with Naringin, a significant decline in MDA levels was observed for 20@PdNPs ($P < 0.01$), 80@PdNPs ($P < 0.05$), and PdNRs ($P < 0.05$). No significant difference in MDA values was observed in rats treated with 1 and 10 μg/kg of PdNPs and cotreated with naringin compared to the control group. Overall, our findings demonstrate that the coadministration of naringin in PdNP-exposed animals effectively suppressed oxidative stress.

3.2.4. Alteration in Inflammatory Markers and Treatment with Naringin. Inflammation in the lungs involves the recruitment and activation of immune cells such as macrophages, neutrophils, and lymphocytes. These cells respond to the pro-inflammatory signals released by apoptotic cells and contribute to the clearance of cellular debris and pathogens.Elevated secretion of pro-inflammatory biomarkers is often associated with the initiation of lung diseases, including pneumonia, fibrosis, chronic obstructive pulmonary disease (COPD), or acute or subacute lung injury.[60,61] Lung injury occurs in two phases, with the first phase involving alveolar damage, microvascular injury, and a cascade of inflammatory events, such as the influx of inflammatory cells and the release of inflammatory mediators. In this study, our focus was on common pro-inflammatory cytokines associated with lung injuries, namely, interleukin (IL)-1β, IL-8, IL-6, and tumor necrosis factor-alpha (TNF-α). These inflammatory mediators can be measured in plasma, serum, or bronchoalveolar lavage fluid (BALF).

IL-1β is a key pro-inflammatory mediator actively present in the early stages of lung injury and serves as a potent inducer of lung damage, including lung fibrosis. It is also responsible for the release of various pro-inflammatory chemokines, such as IL-6, IL-8, macrophage inflammatory protein (MIP)-1α, and monocyte chemotactic protein (MCP)-1.[62,63] Figure 5A shows a dose-dependent upregulation of IL-1β levels following exposure to all three types of PdNPs. Higher doses (10 μg/

https://doi.org/10.1021/acsomega.4c02269
ACS Omega 2024, 9, 32745−32759

kg) of 20@PdNPs, 80@PdNPs, and PdNRs exhibited a statistically significant increase in IL-1β levels compared to the control group rats ($P < 0.01$). However, at lower doses (1 μg/kg) of 20@PdNPs, 80@PdNPs, and PdNRs, only 20@PdNPs showed a statistically significant increase compared to the control group ($P < 0.05$). Co-treatment of the PdNPs-exposed groups with naringin resulted in a slight decrease in IL-1β secretions compared to the untreated PdNPs groups, with the reduction being statistically significant only in rats treated with 10 μg/kg of PdNPs ($P < 0.05$).

IL-8 is a pro-inflammatory chemokine belonging to the cytokine class, which plays a vital role in the chemotaxis of monocytes and neutrophils, guiding these cells to the site of inflammation.[64] Our study observed elevated levels of IL-8 secretion in both the lower ($P < 0.05$) and higher ($P < 0.01$) dose groups of 20@PdNPs, 80@PdNPs, and PdNRs compared to the control group (Figure 6B). Moreover, higher levels of IL-8 secretion were observed in the higher dose group (PdNPs-10) compared to the lower dose group (PdNPs-1). Among all three types of PdNPs, Pd nanorods exhibited the highest levels of IL-8 secretion. Co-treatment with naringin resulted in a reduction in IL-8 levels, although the reduction was statistically significant only in the PdNPs-10 group.

IL-6 is another crucial soluble pro-inflammatory mediator produced in response to infections or tissue damage. Figure 6C represents the concentration of IL-6 in the lungs of female Wistar rats exposed to PdNPs for 28 days. Significantly elevated levels of IL-6 biomarkers were observed in rats treated with 1 μg/kg ($P < 0.01$) and 10 μg/kg of all PdNPs ($P < 0.001$) compared to the control group. In animals dosed with 10 μg/kg of PdNPs, higher levels of IL-6 biomarkers were observed compared to the lower dose group. The difference in IL-6 secretion levels among rats treated with 20@PdNPs, 80@PdNPs, and PdNRs was not statistically significant. Co-treatment with naringin showed a significant reduction in IL-6 levels in both the lower and higher dose groups, indicating the anti-inflammatory effects exhibited by naringin. These findings are consistent with previous studies demonstrating a dose-, size-, and shape-dependent increase in IL-6 secretion.[41,51]

Finally, TNF-α, a pro-inflammatory cytokine, is expressed by alveolar macrophages in the early stages of acute lung injury in response to pathogen stimulation. This cytokine stimulates various other cell signals to recruit immune cells, such as monocytes, neutrophils, and lymphocytes, to the site of inflammation.[65] Our study observed elevated expression of TNF-α biomarkers in the lungs of rats exposed to lower and higher doses of PdNPs (Figure 6D). The difference in TNF-α levels between the control group rats and the PdNP-treated group rats was statistically significant for both doses. Notably, rats treated with a higher dose of PdNPs exhibited higher levels of TNF-α secretion ($P < 0.01$) compared to the lower dose group ($P < 0.05$). Among the PdNPs, 20@PdNPs and PdNRs exhibited higher levels of TNF-α compared to 80 nm-sized PdNPs. A similar observation was reported in our previous in vitro study, where different sizes of spherical and rod-shaped PdNPs were exposed to macrophage cell lines.[51] Co-treatment with an 80 mg/kg dose of naringin resulted in a significant reduction in TNF-α secretions in rats treated with 20@PdNPs, 80@PdNPs, and PdNRs, indicating the anti-inflammatory effects of naringin.

3.2.5. Histological Changes in Lungs. The histopathological examination of a normal lung's alveolar sac constitutes of large air sacs lined with thin blood capillaries (alveolar septa). Within the blood capillaries, cells such as type I pneumocytes, type II pneumocytes, and red blood cells can be

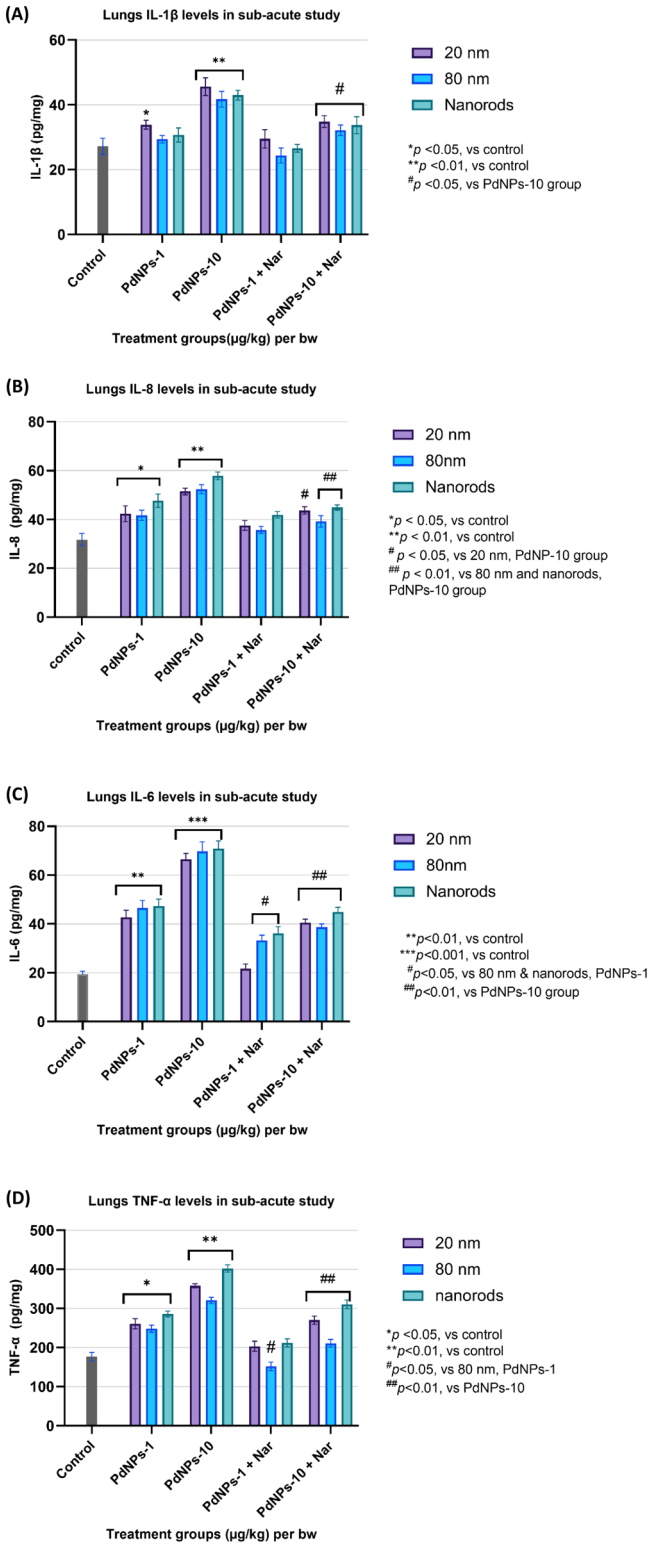

Figure 6. Alteration in pro-inflammatory cytokine levels after 28 days subacute oral treatment with PdNPs of different sizes, shapes, and concentrations and cotreatment with naringin. (A) IL-1β levels in lungs, (B) IL-8 levels in lungs, (C) IL-6 levels in lungs, and (D) TNF-α levels in lungs. Untreated cells were taken as control. Data are expressed as mean ± SD ($n = 5$). Asterisk (*) represents significant differences. Two way-ANOVA, Tukey's multiple comparison test.

https://doi.org/10.1021/acsomega.4c02269
ACS Omega 2024, 9, 32745−32759

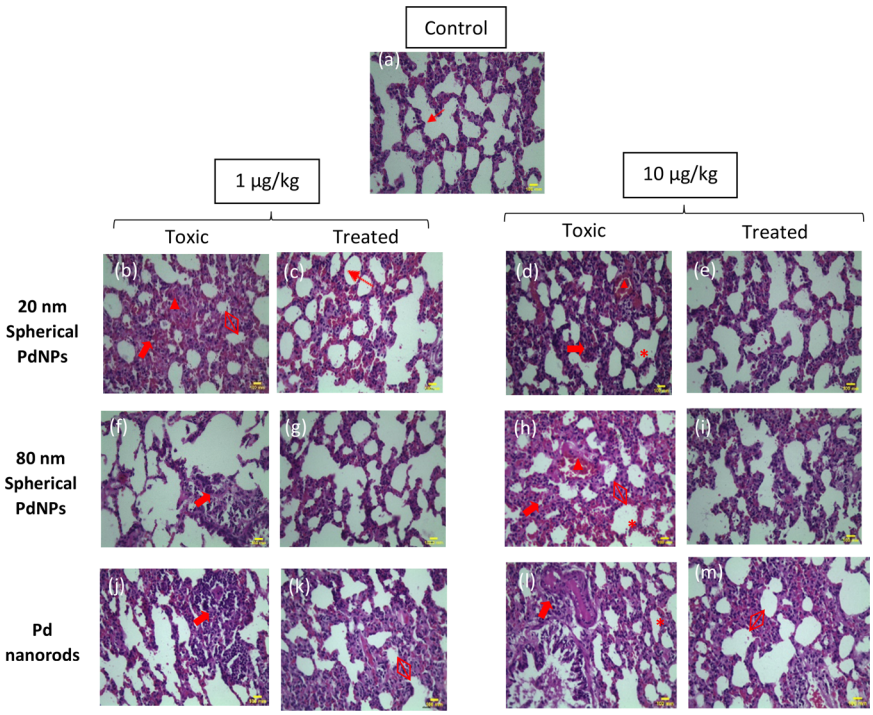

Figure 7. (a) Histological changes in rat lungs of control group showing normal interalveolar septa (↓) and normal alveoli. (b−m) Histological changes in rat lungs induced by PdNPs and naringin where (inverted triangle) signifies hemorrhage, (↔) shows thickening of interalveolar septa, (∗) shows emphysematous changes, and (→) shows mononuclear cell infiltration. Scale bar: 100 mm.

Table 4. Scoring of the Histopathological Alterations in the Lung Tissues of Rats after a 28-Day Subacute Oral Toxicity Study of PdNPs of Different Sizes, Shapes, and Concentrations[a]

group	mononuclear cell infiltration	hemorrhage	thickened alveolar septa	congestion	emphysematous changes	alveolar fibrosis
G1: Control	−	−	−	−	−	−
G2: Pd-NPs, 20 nm, 1 µg/kg	+++	+	+++	+++	+	−
G3: Pd-NPs, 20 nm, 10 µg/kg	+++	++	+++	++	+	−
G4: Pd-NPs, 80 nm, 1 µg/kg	++	−	−	+	−	−
G5: Pd-NPs, 80 nm, 10 µg/kg	++	++	++	++	++	−
G6: Pd-NRs, 1 µg/kg	+	−	+	+	+	−
G7: Pd-NRs, 10 µg/kg	+++	−	+++	+++	++	−
G8:20-PdNPs + Nar, 1 µg/kg	+	−	+	+	−	−
G9:20-PdNPs+ Nar, 10 µg/kg	+	−	+	−	−	−
G10:80-PdNPs+ Nar, 1 µg/kg	+	−	+	−	−	−
G11:80-PdNPs + Nar, 10 µg/kg	+	−	+	−	−	−
G12: PdNRs + Nar, 1 µg/kg	+	−	++	+	+	−
G13: PdNRs+ Nar, 10 µg/kg	++	−	++	−	+	−

[a](−): none, (+): mild, (++) moderate, (+++) severe.

observed. Type I pneumocytes, also known as epithelial cells, constitute the majority (approximately 95%) of lung cells and possess a flat and squamous shape. Conversely, type II pneumocytes exhibit a dome or cuboidal shape.[66,67]

Upon analyzing the histopathological changes in lung tissues, a control group rat displayed a normal alveolar sac in the lung section (Figure 7a). However, rats in groups 2 and 3, administered with 1 µg/kg and 10 µg/kg of 20@PdNPs, exhibited thickened alveolar septa, significant infiltration of macrophages, hemorrhage, and signs of emphysematous changes, indicating the onset of lung inflammation (Figure 7b,d). Conversely, rats in groups 8 and 9, which were cotreated with naringin, displayed milder mononuclear cell infiltration, thinner alveolar septa, and reduced hemorrhage (Figure 7c,e), indicating the potential anti-inflammatory effects of naringin.

Regarding the lung histopathology results of rats in group 4, administered with 1 µg/kg of 80@PdNPs, did not exhibit as severe changes as rats in groups 2, 6, and 7, which were administered 20@PdNPs and PdNRs. Conversely, rats in group 5 (10 µg/kg, 80@PdNPs) displayed more severe changes compared to group 4 (1 µg/kg, 80PdNPs), such as increased macrophage infiltration, congestion, signs of hemorrhage in the air sac, and thickened interalveolar septa (Figure 7f and 7h). Notably, cotreatment with naringin showed noticeable lung recovery, indicating its anti-inflammatory effects (Figure 7g,i).

Histopathological images of rats in groups 6 and 7, administered with 1 and 10 µg/kg of PdNRs, also exhibited various changes in the alveolar sacs of the lungs, including mononuclear cell infiltration, thickened interalveolar septa, and

https://doi.org/10.1021/acsomega.4c02269
ACS Omega 2024, 9, 32745−32759

emphysematous changes (Figure 7j,l). Overall, significant histological changes were induced in the lungs by higher doses of all Pd particles. However, 20@PdNPs exerted significant alterations in lung tissues even at lower doses. Notably, cotreatment with naringin greatly reduced these histological abnormalities in lung tissues. Table 4 shows the scoring of histopathological alterations in lung tissues.

4. CONCLUSIONS

The current investigation illustrates the size and shape-dependent pulmonary toxicity of PdNPs in female Wistar rats, emphasizing the influence of size, shape, and dosage during a 28-day oral exposure. The results of the present study revealed size and shape-dependent alterations in biochemical changes in liver and kidney enzymes, lung oxidative stress, heightened inflammatory markers, and notable histological lung abnormalities, indicating lung injury. These effects were more pronounced on exposure to PdNPs with higher concentrations (10 μg/kg). Notably, PdNPs of 20 nm size exhibited the most severe effects compared to 80 nm PdNPs and PdNRs, likely due to their enhanced ability to circulate in the bloodstream, penetrate tissues, and accumulate in organs, thereby increasing toxicity. Exposure to Pd nanorods also induced substantial oxidative stress, lung inflammation, and alterations in lung histopathology, surpassing the effects observed with 80@PdNPs. Additionally, naringin demonstrated therapeutic potential by ameliorating PdNPs-induced toxicity through the modulation of oxidative and inflammatory pathways.

Given the increasing use of PdNPs in various industrial and biomedical applications, understanding their potential pulmonary toxicity is crucial for risk assessment and occupational health. Moreover, analyzing impact of different size and shape of PdNPs sheds light on the underlying mechanism of lung pathogenies and provides precise risk assessment. Overall, this study provides valuable insights into the underlying mechanisms of PdNPs-induced lung toxicity and underscores the protective effects of naringin in mitigating pulmonary toxicity. By characterizing the toxicity profiles of various PdNP configurations, regulatory agencies and industries can develop targeted guidelines and safety measures. However, further long-term studies of PdNPs exposure on pulmonary health, such as chronic inflammation, fibrosis, or carcinogenicity, are required to have the holistic understanding of toxicity induced by PdNPs. Also, while size and shape are important determinants of nanoparticle behavior, they represent only a subset of the factors influencing toxicity. Other factors, such as surface coating, aggregation state, and exposure duration, also play critical roles and are essential for further studies for the development of safe and sustainable nanotechnology.

■ ASSOCIATED CONTENT

Supporting Information

The Supporting Information is available free of charge at https://pubs.acs.org/doi/10.1021/acsomega.4c02269.

Protocol for antioxidant assay; measurement of superoxide dismutase activity; measurement of catalase activity (CAT); measurement of lipid peroxidation (LPO); measurement of reduced glutathione (GSH); protocol for estimation of cytokine markers by ELISA; estimation of Interluekin-6 (IL-6); estimation of interluekin-8 (IL-8); estimation of interluekin-1β; estimation of TNF-α (PDF)

■ AUTHOR INFORMATION

Corresponding Author

Mohammed Samim − *Department of Chemistry, School of Chemical and Life sciences, Jamia Hamdard, New Delhi 110062, India;* orcid.org/0000-0003-1667-8572; Email: shamim_chem@yahoo.co.in

Authors

Aarzoo − *Department of Chemistry, School of Chemical and Life sciences, Jamia Hamdard, New Delhi 110062, India*

Mobin A. Siddiqui − *Department of Chemistry, School of Chemical and Life sciences, Jamia Hamdard, New Delhi 110062, India*

Mohammad Hasan − *Department of Toxicology, School of Chemical and Life Sciences, Jamia Hamdard, New Delhi 110062, India*

Nidhi − *Centre for Translational & Clinical Research, Jamia Hamdard, New Delhi 110062, India*

Haider A. Khan − *Department of Toxicology, School of Chemical and Life Sciences, Jamia Hamdard, New Delhi 110062, India*

Shweta Rastogi − *Department of Chemistry, Hansraj College, Delhi University, New Delhi 110007, India*

Indu Arora − *Department of Chemistry, Shaheed Rajguru College of Applied Sciences for Women, Delhi University, New Dehli 110062, India*

Complete contact information is available at: https://pubs.acs.org/10.1021/acsomega.4c02269

Author Contributions

Aarzoo: Writing − Original Draft, Writing- Review & Editing, Investigation, Data curation. M.A.S.: Resources, Investigation, Data curation. M.H.: Methodology, Formal analysis. H.A.K.: Resources, Formal analysis. Nidhi: Conceptualization, Project administration. S.R.: Resources. I.A.: Resources. M.S.: Conceptualization, Supervision, Methodology.

Notes

The authors declare no competing financial interest.

The experimental protocol and treatments were approved by the Institutional Animal Ethics Committee (IAEC) of Jamia Hamdard, New Delhi, India (Approval No.1562, registration No. 173/GO/ReBi/S/2000/CPCSEA). All experiments were performed in compliance with the relevant laws of India and institutional guidelines (CPCSEA, IAEC). All rats were handled ethically according to the standard guide for the care and use of laboratory animals. We also declare that this manuscript is our original work, and we have not copied it from anywhere else.

■ ACKNOWLEDGMENTS

The authors would like to express gratitude to the Indian council of medical research (ICMR) for supporting the work with research grant (Grant No. 45/11/2020-Nan/BMS). The Central Animal House facility and TEM facility of SPER, Jamia Hamdard are also gratefully acknowledged for their cooperation and assistance.

■ ABBREVIATIONS

PGMs, platinum group metals; PdNPs, palladium nanoparticles; VEC, vehicle exhaust catalysts; TWC, three-way catalytic converter; (ALT), alanine transaminase; (AST), aspartate transaminase; AST, aspartate transaminase; ALP, alkaline phosphatase

■ REFERENCES

(1) Hans Wedepohl, K. The Composition of the Continental Crust. *Geochim. Cosmochim. Acta* **1995**, *59* (7), 1217−1232.

(2) Kumar, A.; Zhao, Y.; Mohammadi, M. M.; Liu, J.; Thundat, T.; Swihart, M. T. Palladium Nanosheet-Based Dual Gas Sensors for Sensitive Room-Temperature Hydrogen and Carbon Monoxide Detection. *ACS Sens.* **2022**, *7* (1), 225−234.

(3) Lebaschi, S.; Hekmati, M.; Veisi, H. Green Synthesis of Palladium Nanoparticles Mediated by Black Tea Leaves (Camellia Sinensis) Extract: Catalytic Activity in the Reduction of 4-Nitrophenol and Suzuki-Miyaura Coupling Reaction under Ligand-Free Conditions. *J. Colloid Interface Sci.* **2017**, *485*, 223−231.

(4) Samim, M.; Aarzoo. 16 - Hyaluronic Acid-Magnetic Nanocomposites for Gene Delivery. *Polysaccharide-Based Nanocompos. Gene Delivery Tissue Eng.* **2021**, 311−323.

(5) Vijilvani, C.; Bindhu, M. R.; Frincy, F. C.; AlSalhi, M. S.; Sabitha, S.; Saravanakumar, K.; Devanesan, S.; Umadevi, M.; Aljaafreh, M. J.; Atif, M. Antimicrobial and Catalytic Activities of Biosynthesized Gold, Silver and Palladium Nanoparticles from Solanum Nigurum Leaves. *Journal of Photochemistry and Photobiology B: Biology* **2020**, *202*, No. 111713.

(6) Matthey, J. *PGM Market Report* 2022; p 60. https://matthey.com/documents/161599/509428/PGM-market-report-May-2022.pdf/542bcada-f4ac-a673-5f95-ad1bbfca5106?t=1655877358676.

(7) Heck, R. M.; Farrauto, R. J. Automobile Exhaust Catalysts. *Applied Catalysis A: General* **2001**, *221* (1−2), 443−457.

(8) Aarzoo; Nidhi; Samim, M. Palladium Nanoparticles as Emerging Pollutants from Motor Vehicles: An in-Depth Review on Distribution, Uptake and Toxicological Effects in Occupational and Living Environment. *Science of The Total Environment* **2022**, *823*, No. 153787.

(9) Balaram, V. Environmental Impact of Platinum, Palladium, and Rhodium Emissions from Autocatalytic Converters − A Brief Review of the Latest Developments. In *Handbook of Environmental Materials Management*; Hussain, C. M., Ed.; Springer International Publishing: Cham, 2020; pp 1−37. DOI: 10.1007/978-3-319-58538-3_194-1.

(10) *Palladium Emissions in the Environment*; Zereini, F.; Alt, F., Eds.; Springer Berlin Heidelberg: Berlin, Heidelberg, 2006. DOI: 10.1007/3-540-29220-9.

(11) Barbante, C.; Veysseyre, A.; Ferrari, C.; Van De Velde, K.; Morel, C.; Capodaglio, G.; Cescon, P.; Scarponi, G.; Boutron, C. Greenland Snow Evidence of Large Scale Atmospheric Contamination for Platinum, Palladium, and Rhodium. *Environ. Sci. Technol.* **2001**, *35* (5), 835−839.

(12) Bernardino, C. A. R.; Mahler, C. F.; Santelli, R. E.; Braz, B. F.; Borges, R. C.; Fernandes, J. O.; Gomes, A. C. S.; Cincotto, F. H.; Novo, L. A. B. Contamination of Roadside Soils by Metals Linked to Catalytic Converters in Rio De Janeiro, Brazil. *Environ. Forensics* **2021**, *23*, 221−233.

(13) Jackson, M.; Sampson, J.; Prichard, H. Platinum and Palladium Variations through the Urban Environment: Evidence from 11 Sample Types from Sheffield. *UK. Science of The Total Environment* **2007**, *385* (1−3), 117−131.

(14) Komendova, R. The HR-CS-GF-AAS Determination and Preconcentration of Palladium in Contaminated Urban Areas. *Especially in Lichens. Environmental Pollution* **2020**, *256*, No. 113468.

(15) Omrani, M.; Goriaux, M.; Jean-Soro, L.; Ruban, V. Platinum Group Elements in Atmospheric PM10 Particles and Dry Deposition in France. *Environ. Sci. Pollut Res.* **2021**, *28* (25), 33231−33240.

(16) Özen, M.; Özen, S. A.; ÇeviK, U. Vehicular and Industrial Sources of PGEs, Au and Ce in Surface Soil and Roadside Soils and Dusts from Two Cities of Turkey. *Sakarya Univ. J. Sci.* **2021**, *25* (2), 484−497.

(17) Wiseman, C. L. S.; Zereini, F. Airborne Particulate Matter, Platinum Group Elements and Human Health: A Review of Recent Evidence. *Science of The Total Environment* **2009**, *407* (8), 2493−2500.

(18) Zereini, F.; Alt, F.; Messerschmidt, J.; von Bohlen, A.; Liebl, K.; Püttmann, W. Concentration and Distribution of Platinum Group Elements (Pt, Pd, Rh) in Airborne Particulate Matter in Frankfurt Am Main, Germany. *Environ. Sci. Technol.* **2004**, *38* (6), 1686−1692.

(19) Prichard, H. M.; Fisher, P. C. Identification of Platinum and Palladium Particles Emitted from Vehicles and Dispersed into the Surface Environment. *Environ. Sci. Technol.* **2012**, *46* (6), 3149−3154.

(20) El-Seedi, H. R.; El-Shabasy, R. M.; Khalifa, S. A. M.; Saeed, A.; Shah, A.; Shah, R.; Iftikhar, F. J.; Abdel-Daim, M. M.; Omri, A.; Hajrahand, N. H.; Sabir, J. S. M.; Zou, X.; Halabi, M. F.; Sarhan, W.; Guo, W. Metal Nanoparticles Fabricated by Green Chemistry Using Natural Extracts: Biosynthesis, Mechanisms, and Applications. *RSC Adv.* **2019**, *9* (42), 24539−24559.

(21) Abdel-Daim, M. M.; Eissa, I. A. M.; Abdeen, A.; Abdel-Latif, H. M. R.; Ismail, M.; Dawood, M. A. O.; Hassan, A. M. Lycopene and Resveratrol Ameliorate Zinc Oxide Nanoparticles-Induced Oxidative Stress in Nile Tilapia, Oreochromis Niloticus. *Environmental Toxicology and Pharmacology* **2019**, *69*, 44−50.

(22) Rahman, Md. M.; Bibi, S.; Rahaman, Md. S.; Rahman, F.; Islam, F.; Khan, M. S.; Hasan, M. M.; Parvez, A.; Hossain, Md. A.; Maeesa, S. K.; Islam, Md. R.; Najda, A.; Al-malky, H. S.; Mohamed, H. R. H.; AlGwaiz, H. I. M.; Awaji, A. A.; Germoush, M. O.; Kensara, O. A.; Abdel-Daim, M. M.; Saeed, M.; Kamal, M. A. Natural Therapeutics and Nutraceuticals for Lung Diseases: Traditional Significance, Phytochemistry, and Pharmacology. *Biomedicine & Pharmacotherapy* **2022**, *150*, No. 113041.

(23) Zahin, N.; Anwar, R.; Tewari, D.; Kabir, Md. T.; Sajid, A.; Mathew, B.; Uddin, Md. S.; Aleya, L.; Abdel-Daim, M. M. Nanoparticles and Its Biomedical Applications in Health and Diseases: Special Focus on Drug Delivery. *Environ. Sci. Pollut Res.* **2020**, *27* (16), 19151−19168.

(24) Schäfer, J.; Hannker, D.; Eckhardt, J.-D.; Stüben, D. Uptake of Traffic-Related Heavy Metals and Platinum Group Elements (PGE) by Plants. *Science of The Total Environment* **1998**, *215* (1−2), 59−67.

(25) Morton, O.; Puchelt, H.; Hernández, E.; Lounejeva, E. Traffic-Related Platinum Group Elements (PGE) in Soils from Mexico City. *Journal of Geochemical Exploration* **2001**, *72* (3), 223−227.

(26) Janssen, N. A. H.; Brunekreef, B.; van Vliet, P.; Aarts, F.; Meliefste, K.; Harssema, H.; Fischer, P. The Relationship between Air Pollution from Heavy Traffic and Allergic Sensitization, Bronchial Hyperresponsiveness, and Respiratory Symptoms in Dutch Schoolchildren. *Environ. Health Perspect* **2003**, *111* (12), 1512−1518.

(27) *Pollutants in Urban Waste Water and Sewage Sludge*. EC, 2001, 273.

(28) Göbel, P.; Dierkes, C.; Coldewey, W. G. Storm Water Runoff Concentration Matrix for Urban Areas. *Journal of Contaminant Hydrology* **2007**, *91* (1−2), 26−42.

(29) Wilkinson, K. E.; Palmberg, L.; Witasp, E.; Kupczyk, M.; Feliu, N.; Gerde, P.; Seisenbaeva, G. A.; Fadeel, B.; Dahlén, S.-E.; Kessler, V. G. Solution-Engineered Palladium Nanoparticles: Model for Health Effect Studies of Automotive Particulate Pollution. *ACS Nano* **2011**, *5* (7), 5312−5324.

(30) Ji, J.; Hedelin, A.; Malmlöf, M.; Kessler, V.; Seisenbaeva, G.; Gerde, P.; Palmberg, L. Development of Combining of Human Bronchial Mucosa Models with XposeALI for Exposure of Air Pollution Nanoparticles. *PLoS One* **2017**, *12* (1), No. e0170428.

(31) Kabir, M. T.; Rahman, M. H.; Shah, M.; Jamiruddin, M. R.; Basak, D.; Al-Harrasi, A.; Bhatia, S.; Ashraf, G. M.; Najda, A.; El-kott, A. F.; Mohamed, H. R. H.; Al-malky, H. S.; Germoush, M. O.; Altyar, A. E.; Alwafai, E. B.; Ghaboura, N.; Abdel-Daim, M. M. Therapeutic Promise of Carotenoids as Antioxidants and Anti-Inflammatory Agents in Neurodegenerative Disorders. *Biomed. Pharmacother.* **2022**, *146*, No. 112610.

https://doi.org/10.1021/acsomega.4c02269
ACS Omega 2024, 9, 32745−32759

(32) Kabir, Md. T.; Rahman, Md. H.; Akter, R.; Behl, T.; Kaushik, D.; Mittal, V.; Pandey, P.; Akhtar, M. F.; Saleem, A.; Albadrani, G. M.; Kamel, M.; Khalifa, S. A. M.; El-Seedi, H. R.; Abdel-Daim, M. M. Potential Role of Curcumin and Its Nanoformulations to Treat Various Types of Cancers. *Biomolecules* **2021**, *11* (3), 392.
(33) Labib, R.; Youssef, F.; Ashour, M.; Abdel-Daim, M.; Ross, S. Chemical Composition of Pinus Roxburghii Bark Volatile Oil and Validation of Its Anti-Inflammatory Activity Using Molecular Modelling and Bleomycin-Induced Inflammation in Albino Mice. *Molecules* **2017**, *22* (9), 1384.
(34) Tang, Y.; Edelmann, R. E.; Zou, S. Length Tunable Penta-Twinned Palladium Nanorods: Seedless Synthesis and Electro-oxidation of Formic Acid. *Nanoscale* **2014**, *6* (11), 5630.
(35) Clause, B. T. The Wistar Rat as a Right Choice: Establishing Mammalian Standards and the Ideal of a Standardized Mammal. *J. Hist Biol.* **1993**, *26* (2), 329−349.
(36) Filon, F. L.; Uderzo, D.; Bagnato, E. Sensitization to Palladium Chloride: A 10-Year Evaluation. *American Journal of Contact Dermatitis* **2003**, *14* (2), 78−81.
(37) Muris, J.; Goossens, A.; Gonçalo, M.; Bircher, A. J.; Giménez-Arnau, A.; Foti, C.; Rustemeyer, T.; Feilzer, A. J.; Kleverlaan, C. J. Sensitization to Palladium and Nickel in Europe and the Relationship with Oral Disease and Dental Alloys: Pd AND Ni SENSITIZATION: DENTAL ALLOYS AND ORAL DISEASE. *Contact Dermatitis* **2015**, *72* (5), 286−296.
(38) Fontana, L.; Leso, V.; Marinaccio, A.; Cenacchi, G.; Papa, V.; Leopold, K.; Schindl, R.; Bocca, B.; Alimonti, A.; Iavicoli, I. The Effects of Palladium Nanoparticles on the Renal Function of Female Wistar Rats. *Nanotoxicology* **2015**, *9* (7), 843−851.
(39) Iavicoli, I.; Fontana, L.; Leso, V.; Corbi, M.; Marinaccio, A.; Leopold, K.; Schindl, R.; Lucchetti, D.; Calapà, F.; Sgambato, A. Subchronic Exposure to Palladium Nanoparticles Affects Serum Levels of Cytokines in Female Wistar Rats. *Hum Exp Toxicol* **2018**, *37* (3), 309−320.
(40) Cristaudo, A.; Bordignon, V.; Petrucci, F.; Caimi, S.; De Rocco, M.; Picardo, M.; Fei, P. C.; Ensoli, F. Release of Palladium from Biomechanical Prostheses in Body Fluids Can Induce or Support PD-Specific IFNγ T Cell Responses and the Clinical Setting of a Palladium Hypersensitivity. *Int. J. Immunopathol Pharmacol* **2009**, *22* (3), 605−614.
(41) Iavicoli, I.; Fontana, L.; Corbi, M.; Leso, V.; Marinaccio, A.; Leopold, K.; Schindl, R.; Sgambato, A. Exposure to Palladium Nanoparticles Affects Serum Levels of Cytokines in Female Wistar Rats. *PLoS One* **2015**, *10* (11), No. e0143801.
(42) Aarzoo; Naqvi, S.; Agarwal, N. B.; Singh, M. P.; Samim, M. Bio-Engineered Palladium Nanoparticles: Model for Risk Assessment Study of Automotive Particulate Pollution on Macrophage Cell Lines. *RSC Adv.* **2021**, *11* (3), 1850−1861.
(43) Bernardino, C. A. R.; Mahler, C. F.; Santelli, R. E.; Braz, B. F.; Borges, R. C.; Fernandes, J. O.; Gomes, A. C. S.; Cincotto, F. H.; Novo, L. A. B. Contamination of Roadside Soils by Metals Linked to Catalytic Converters in Rio De Janeiro, Brazil. *Environ. Forensics* **2021**, *23*, 221−233.
(44) Vasile, G. G.; Dinu, C.; Kim, L.; Tenea, A.; Simion, M.; Ene, C.; Spinu, C.; Ungureanu, E.-M.; Manolache, D. Platinum Group Elements in Road Dust and Vegetation from Some European and National Roads with Intensive Car Traffic in Romania. *Rev. Chim.* **2019**, *70* (1), 286−292.
(45) Ghanbari-Movahed, M.; Jackson, G.; Farzaei, M. H.; Bishayee, A. A Systematic Review of the Preventive and Therapeutic Effects of Naringin Against Human Malignancies. *Front. Pharmacol.* **2021**, *12*, No. 639840.
(46) Kim, J. K.; Park, J. H.; Ku, H. J.; Kim, S. H.; Lim, Y. J.; Park, J. W.; Lee, J. H. Naringin Protects Acrolein-Induced Pulmonary Injuries through Modulating Apoptotic Signaling and Inflammation Signaling Pathways in Mice. *J. Nutr Biochem* **2018**, *59*, 10−16.
(47) Liu, Y.; Wu, H.; Nie, Y.; Chen, J.; Su, W.; Li, P. Naringin Attenuates Acute Lung Injury in LPS-Treated Mice by Inhibiting NF-κB Pathway. *International Immunopharmacology* **2011**, *11* (10), 1606−1612.
(48) Lowry, O.; Rosebrough, N.; Farr, A. L.; Randall, R. PROTEIN MEASUREMENT WITH THE FOLIN PHENOL REAGENT. *J. Biol. Chem.* **1951**, *193* (1), 265−275.
(49) Pearse, A. G. E. *Histochemistry, Theoretical and Applied*, 2nd ed.; Little Brown and Company: Boston, 1968; Vol. 2.
(50) Humason, G. L. *Animal Tissue Techniques*, 4th ed.; W. H. Freeman & Co.: San Francisco, 1979.
(51) Aarzoo; Nematullah, M.; Siddiqui, M. A.; Nidhi; khan, F.; Samim, M. Synthesis and Characterization of Palladium Nanoparticles by Varying Size, Shape and Synthetic Approach: A Comparative Risk Assessment Study in-Vitro as a Step towards the Development of Safe and Sustainable Nanotechnology. *Atmospheric Pollution Research* **2022**, *13* (8), No. 101505.
(52) Tahir, K.; Nazir, S.; Ahmad, A.; Li, B.; Ali Shah, S. A.; Khan, A. U.; Khan, G. M.; Khan, Q. U.; Haq Khan, Z. U.; Khan, F. U. Biodirected Synthesis of Palladium Nanoparticles Using Phoenix Dactylifera Leaves Extract and Their Size Dependent Biomedical and Catalytic Applications. *RSC Adv.* **2016**, *6* (89), 85903−85916.
(53) Khan, M.; Albalawi, G. H.; Shaik, M. R.; Khan, M.; Adil, S. F.; Kuniyil, M.; Alkhathlan, H. Z.; Al-Warthan, A.; Siddiqui, M. R. H. Miswak Mediated Green Synthesized Palladium Nanoparticles as Effective Catalysts for the Suzuki Coupling Reactions in Aqueous Media. *Journal of Saudi Chemical Society* **2017**, *21* (4), 450−457.
(54) Tagde, P.; Tagde, P.; Islam, F.; Tagde, S.; Shah, M.; Hussain, Z. D.; Rahman, Md. H.; Najda, A.; Alanazi, I. S.; Germoush, M. O.; Mohamed, H. R. H.; Algandaby, M. M.; Nasrullah, M. Z.; Kot, N.; Abdel-Daim, M. M. The Multifaceted Role of Curcumin in Advanced Nanocurcumin Form in the Treatment and Management of Chronic Disorders. *Molecules* **2021**, *26* (23), 7109.
(55) Alarifi, S.; Ali, D.; Alkahtani, S.; Almeer, R. S. ROS-Mediated Apoptosis and Genotoxicity Induced by Palladium Nanoparticles in Human Skin Malignant Melanoma Cells. *Oxidative Medicine and Cellular Longevity* **2017**, *2017*, 1−10.
(56) Younus, H. Therapeutic Potentials of Superoxide Dismutase. *Int. J. Health Sci.* **2018**, *12* (3), 88−93.
(57) Forman, H. J.; Zhang, H.; Rinna, A. Glutathione: Overview of Its Protective Roles, Measurement, and Biosynthesis. *Mol. Aspects Med.* **2009**, *30* (1−2), 1−12.
(58) Aquilano, K.; Baldelli, S.; Ciriolo, M. R. Glutathione: New Roles in Redox Signaling for an Old Antioxidant. *Front. Pharmacol.* **2014**, *5*, 196 DOI: 10.3389/fphar.2014.00196.
(59) Sukhanova, A.; Bozrova, S.; Sokolov, P.; Berestovoy, M.; Karaulov, A.; Nabiev, I. Dependence of Nanoparticle Toxicity on Their Physical and Chemical Properties. *Nanoscale Res. Lett.* **2018**, *13* (1), 44.
(60) Kany, S.; Vollrath, J. T.; Relja, B. Cytokines in Inflammatory Disease. *IJMS* **2019**, *20* (23), 6008.
(61) Grewal, A. K.; Singh, T. G.; Sharma, D.; Sharma, V.; Singh, M.; Rahman, Md. H.; Najda, A.; Walasek-Janusz, M.; Kamel, M.; Albadrani, G. M.; Akhtar, M. F.; Saleem, A.; Abdel-Daim, M. M. Mechanistic Insights and Perspectives Involved in Neuroprotective Action of Quercetin. *Biomedicine & Pharmacotherapy* **2021**, *140*, No. 111729.
(62) Pirela, S. V.; Bhattacharya, K.; Wang, Y.; Zhang, Y.; Wang, G.; Christophi, C. A.; Godleski, J.; Thomas, T.; Qian, Y.; Orandle, M. S.; Sisler, J. D.; Bello, D.; Castranova, V.; Demokritou, P. A 21-Day Sub-Acute, Whole-Body Inhalation Exposure to Printer-Emitted Engineered Nanoparticles in Rats: Exploring Pulmonary and Systemic Effects. *NanoImpact* **2019**, *15*, No. 100176.
(63) Siddiqui, M. A.; Akhter, J.; Aarzoo; Junaid Bashir, D.; Manzoor, S.; Rastogi, S.; Arora, I.; Aggarwal, N. B.; Samim, M. Resveratrol Loaded Nanoparticles Attenuate Cognitive Impairment and Inflammatory Markers in PTZ-Induced Kindled Mice. *International Immunopharmacology* **2021**, *101*, No. 108287.
(64) Allen, T. C.; Kurdowska, A. Interleukin 8 and Acute Lung Injury. *Archives of Pathology & Laboratory Medicine* **2014**, *138* (2), 266−269.

https://doi.org/10.1021/acsomega.4c02269
ACS Omega 2024, 9, 32745−32759

(65) Xu, S.; Xiaojing, L.; Xinyue, S.; Wei, C.; Honggui, L.; Shiwen, X. Pig Lung Fibrosis Is Active in the Subacute CdCl2 Exposure Model and Exerts Cumulative Toxicity through the M1/M2 Imbalance. *Ecotoxicology and Environmental Safety* **2021**, *225*, No. 112757.
(66) Bouakkaz, I.; Khelili, K.; Rebai, T.; Lock, A. Pulmonary Toxicity Induced by N-Hexane in Wistar Male Rats After Oral Subchronic Exposure. *Dose-Response* **2018**, *16* (4), No. 155932581879956.
(67) Yu, Y.; Zhu, T.; Li, Y.; Jing, L.; Yang, M.; Li, Y.; Duan, J.; Sun, Z. Repeated Intravenous Administration of Silica Nanoparticles Induces Pulmonary Inflammation and Collagen Accumulation via JAK2/STAT3 and TGF-β/Smad3 Pathways in Vivo. *IJN* **2019**, *14*, 7237−7247.

https://doi.org/10.1021/acsomega.4c02269
ACS Omega 2024, 9, 32745−32759